International Journal of Computational Methods
Vol. 14, No. 5 (2017) 1750052 (19 pages)

DOI: 10.1142/S0219876217500529

An Enriched Edge-Based Smoothed FEM for Linear Elastic Fracture Problems

Yongtao Yang*, Hong Zheng†,‡ and Xiuli Du†

*State Key Laboratory of Geomechanics and Geotechnical Engineering
Institute of Rock and Soil Mechanics, Chinese Academy of Sciences
Wuhan 430071, P. R. China

†Key Laboratory of Urban Security and Disaster Engineering
Ministry of Education, Beijing University of Technology
Beijing 100124, P. R. China
‡hzheng@whrsm.ac.cn

Accepted 8 October 2016
Published 1 November 2016

Based on the edge-based smoothed FEM (ES-FEM) and the partition of unity, the first major items of Williams' series for the displacement field near the crack tip are incorporated in the test and trial function space, resulting in the enriched ES-FEM formulation, eEF-FEM. The eES-FEM does not differentiate any shape functions, avoiding the treatment of the $1/r$ singularity in computing the stiffness matrix. The complexity of computation is accordingly reduced. Meanwhile, it is pointed out that the variational foundation of the eES-FEM is the generalized Galerkin method. Typical numerical examples are analyzed, suggesting that the results of the eES-FEM are much better than either FEM or ES-FEM.

Keywords: Finite element method (FEM); edge-based smoothed FEM (ES-FEM); enriched edge-based smoothed FEM (eES-FEM); stress intensity factors (SIFs); generalized Galerkin method.

1. Introduction

The fracture behavior of cracked brittle structures, such as hard rocks, depends greatly upon the stress and strain in the vicinity of the crack tip [Jiang *et al.* (2011)]. In linear elastic fracture mechanics, the stress intensity factor (SIF) characterizes the singularity strength of the displacement and stress distribution around the crack tip, and plays the most important role in the failure analysis [Liu *et al.* (2011a)]. In general, however, the analytical solutions for SIFs are difficult to obtain. Therefore, many effective numerical methods such as the finite element methods (FEM) [Zienkiewicz and Taylor (2000)], the boundary element methods [Yan (2007); Leonel

et al. (2012)], the mesh-less methods [Brighenti (2005); Duflot and Nguyen-Dang (2004)], the extended finite element method (XFEM) [Sukumar *et al.* (2003); Zheng *et al.* (2015)], and the numerical manifold method (NMM) [Zheng and Xu (2014)] have been proposed.

FEM is currently the most commonly used numerical method in solving problems from science and engineering. But it suffers from two obvious shortcomings. One is overly stiff, leading to underestimation of the solution in the energy norm, and the other is the significant loss of accuracy if heavily distorted elements exist in the mesh [Liu *et al.* (2011a)].

Groups of mesh-less methods are also developed for fracture problems [Brighenti (2005); Duflot and Nguyen-Dang (2004)], where the trial and test functions can be constructed without reliance on element meshes. With the complex construction of the trial and test functions, however, mesh-less methods have inherent shortcomings in the stability and efficiency of numerical integration [Puso *et al.* (2008)]. In addition, extra difficulties exist in treating the essential boundary conditions due to the absence of the Kronecker delta property of the shape functions [Zheng *et al.* (2010)].

The XFEM and the generalized finite element method (GFEM), which are both within the framework of partition of unity, are versatile in the analysis of problems characterized by discontinuities, singularities, localized deformations and complex geometries [Sukumar *et al.* (2003); Belytschko *et al.* (2009)]. Used to describe complicated crack geometry, the level set method has become an important ingredient of XFEM (GFEM), particular in three-dimensional cases. However, it should be mentioned that in the application of level sets to cracks, the update of level sets still poses difficulties, see details in Belytschko *et al.* [2009].

Recently, a family of smoothed finite element methods (S-FEMs) [Liu and Nguyen-Thoi (2010)] relied on the strain smoothing technique [Chen *et al.* (2001)] have been developed for a wide range of practical problems, such as plates and shells [Nguyen-Xuan *et al.* (2008); Nguyen-Thanh *et al.* (2008)], piezoelectricity [Nguyen-Xuan *et al.* (2009)], fracture mechanics [Jiang *et al.* (2011); Liu and Nguyen-Thoi (2010); Liu *et al.* (2011a,b)] and viscoelastoplasticity [Nguyen-Thoi *et al.* (2009)]. The S-FEM can adopt the same mesh as the standard FEM, although more flexible meshes are allowable, to approximate the field variable of interest, but the gradient of the field variable is computed by a smoothing process rather than differentiating operations. Depending on the way that smoothing domains are created, the S-FEMs have different features and properties. There are four modes in the S-FEM: cell-based S-FEM (CS-FEM), node-based S-FEM (NS-FEM), edge-based S-FEM (ES-FEM) and face-based S-FEM (FS-FEM) [Liu and Nguyen-Thoi (2010)]. Intuitively, applying the strain smoothing technique on smoothing domains helps soften the over-stiffness of the standard FEM model, and hence improves the accuracy of solutions in both displacement and stress [Nguyen-Xuan *et al.* (2012)]. Among these S-FEM models, the ES-FEM has been found so far the most computationally efficient [Liu and Nguyen-Thoi (2010)].

In this study, the ES-FEM interpolation is augmented by the major items of Williams' displacement series in the vicinity of a crack tip to reflect the asymptotic behavior of the solution near the crack tip, leading to the enriched edge-based smoothed FEM (eES-FEM). The formulation of eES-FEM only involves the shape functions with no need to calculate their derivatives in forming the element stiffness matrix, and the $1/r$ singularity at the crack tip is accordingly removed. Some typical examples are analyzed to examine the performance of the eES-FEM, and comparisons with FEM and ES-FEM are made. The numerical results indicate that the results from eES-FEM are far more accurate than either FEM or ES-FEM.

2. Brief on Problem

Consider a 2D linear elastic problem defined on domain Ω bounded by $\partial\Omega = \Gamma_u \cup \Gamma_t \cup \Gamma_c$, as shown in Fig. 1. Here, Γ_u is the displacement boundary; Γ_t the traction boundary; and Γ_c the crack surface, defined by $\Gamma_c = \Gamma_{c^+} \cup \Gamma_{c^-}$; with Γ_{c^+} and Γ_{c^-} the upper and lower crack surfaces, respectively. The governing equations and the boundary conditions for this problem are as follows:

(1) the equilibrium equations

$$\nabla \cdot \boldsymbol{\sigma} + \boldsymbol{b} = 0 \quad \text{in } \Omega, \tag{1}$$

where $\boldsymbol{\sigma}$ is the Cauchy stress, and $\boldsymbol{b}$ the body force per unit volume;

(2) the constitutive equation

$$\boldsymbol{\sigma} = \boldsymbol{D}\boldsymbol{\varepsilon} \quad \text{in } \Omega, \tag{2}$$

where $\boldsymbol{D}$ is the Hooke matrix of elastic constants and $\boldsymbol{\varepsilon}$ the strain;

(3) the compatibility equation

$$\boldsymbol{\varepsilon} = \partial \boldsymbol{u} \quad \text{in } \Omega, \tag{3}$$

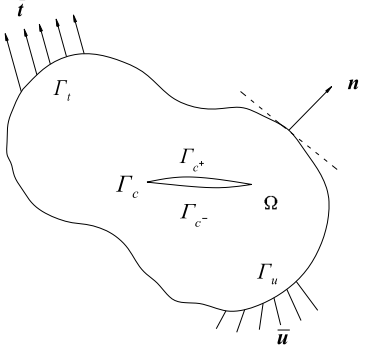

Fig. 1. A 2D linear elastic cracked body.

where $\boldsymbol{u}$ is the displacement vector, and ∂ a matrix of differential operators

$$\partial = \begin{bmatrix} \dfrac{\partial}{\partial x} & 0 & \dfrac{\partial}{\partial y} \\ 0 & \dfrac{\partial}{\partial y} & \dfrac{\partial}{\partial x} \end{bmatrix}^T ; \tag{4}$$

(4) and the boundary conditions

$$\boldsymbol{\sigma} \cdot \boldsymbol{n} = \overline{\boldsymbol{t}} \quad \text{on } \Gamma_t, \tag{5}$$

$$\boldsymbol{\sigma} \cdot \boldsymbol{n} = 0 \quad \text{on } \Gamma_c, \tag{6}$$

$$\boldsymbol{u} = \overline{\boldsymbol{u}} \quad \text{on } \Gamma_u, \tag{7}$$

where $\boldsymbol{n}$ is the unit outward normal, $\overline{\boldsymbol{t}}$ and $\overline{\boldsymbol{u}}$ are the prescribed traction vector on Γ_t and displacement vector on Γ_u, respectively.

3. The eES-FEM Formulation

3.1. *The approximation of displacements based on the partition of unity*

In the partition of unity method (PUM) [Babuška and Melenk (1997); Melenk and Babuška (1996)], we cover the problem domain Ω with a group of patches, denoted by $\{\omega_i\}$. Here, each ω_i is a simply connected domain. If a finite element mesh is used to form $\{\omega_i\}, \omega_i$ can be the collection of all elements sharing node-i, referred to as the star in the literature. Over ω_i, we define a function space in which the functions can reflect the asymptotic behavior of solutions over ω_i.

In this study, we stipulate that the cracks match with the mesh. Purely for the simplicity in programming, such a stipulation avoids complicated element cutting, but it is by no means essential and can be discarded as in XFEM or NMM [Zheng and Xu (2014)].

If node-i is a crack tip, we select local functions over ω_i having the form,

$$\boldsymbol{u}_i(\boldsymbol{x}) = \boldsymbol{P}_{it}(\boldsymbol{x}) \cdot \boldsymbol{a}_{it} \tag{8}$$

with

$$\boldsymbol{P}_{it}(\boldsymbol{x}) = \begin{bmatrix} 1 & 0 & \Phi_1 & 0 & \Phi_2 & 0 & \Phi_3 & 0 & \Phi_4 & 0 \\ 0 & 1 & 0 & \Phi_1 & 0 & \Phi_2 & 0 & \Phi_3 & 0 & \Phi_4 \end{bmatrix}, \tag{9}$$

where $\boldsymbol{a}_{it}$ are the unknown coefficient vector of sixth order, referred to as the generalized degrees of freedom vector in the finite element literature. And $\Phi_i, i = 1, \ldots, 4$,

$$\begin{bmatrix} \Phi_1 & \Phi_2 & \Phi_3 & \Phi_4 \end{bmatrix} = \begin{bmatrix} \sqrt{r}\sin\dfrac{\theta}{2} & \sqrt{r}\cos\dfrac{\theta}{2} & \sqrt{r}\sin\dfrac{3\theta}{2} & \sqrt{r}\cos\dfrac{3\theta}{2} \end{bmatrix} \tag{10}$$

are the first four items of Williams' displacement series [Williams (1957)], where (r, θ) is the polar coordinate in the local coordinate system with the origin at the crack tip.

If node-i is an ordinary node, the local function over ω_i are

$$\boldsymbol{u}_i(\boldsymbol{x}) = \boldsymbol{P}_{io}(\boldsymbol{x}) \cdot \boldsymbol{a}_{io} \tag{11}$$

with

$$\boldsymbol{P}_{io}(\boldsymbol{x}) = \begin{bmatrix} 1 & 0 \\ 0 & 1 \end{bmatrix} \tag{12}$$

and

$$\boldsymbol{a}_{io} = (u_i \quad v_i)^T \tag{13}$$

in which u_i and v_i are the displacement components of node-i in the x-axis and y-axis, respectively.

In eES-FEM, only the asymptotic near-tip displacement field (or first major items of Williams' series) which has been adopted by XFEM for the displacement field near the crack tip are incorporated in the local approximation for the crack tip node. However, the step function for the discontinuity of the interior of a crack is not incorporated in the current code. We will incorporate the step function in eES-FEM in our future work, so as to make a wide application for eES-FEM.

Associated with ω_i is the weight function $\varphi_i(\boldsymbol{x})$, which composes of all shape functions of all elements at node-i. Outside $\omega_i, \varphi_i(\boldsymbol{x}) = 0$. So, $\{\varphi_i(\boldsymbol{x})\}$ constitutes the partition of unity subordinate to $\{\omega_i\}$.

For the simplicity of presentation, we partition Ω with a triangular mesh. Taking a typical element $\Omega^e$of the mesh with node indices 1, 2 and 3, the approximation to displacement vector $\boldsymbol{u}(x, y)$ in Ω^e is expressed by

$$\boldsymbol{u} = \sum_{i=1}^{3} \varphi_i u_i = \sum_{i=1}^{3} L_i u_i \tag{14}$$

due to the compact support property of $\{\varphi_i(\boldsymbol{x})\}$. Here, $\varphi_i = L_i =$ area coordinate of node-i of triangle Ω^e, see Zienkiewicz and Taylor [2000] for details.

By substituting Eq. (8) or (11) into Eq. (14), we have the matrix form equivalent to Eq. (14)

$$\boldsymbol{u} = \boldsymbol{N}\boldsymbol{a}^e, \tag{15}$$

where $\boldsymbol{a}^e =$ generalized degrees of freedom vector collecting generalized degrees of freedom of three nodes of Ω^e; $\boldsymbol{N} = [\boldsymbol{N}_1 \ \boldsymbol{N}_2 \ \boldsymbol{N}_3 \ ]$, defined by

$$\boldsymbol{N}_i = L_i \boldsymbol{P}_i \tag{16}$$

with $i = 1, 2, 3$; $\boldsymbol{P}_i = \boldsymbol{P}_{io}$ if node-i is an ordinary node; or $\boldsymbol{P}_i = \boldsymbol{P}_{it}$ if node-i is a crack tip.

In eES-FEM, only the crack tip node is enriched with the asymptotic near-tip displacement field and no extra nodes are needed to reproduce the stress singularity in the vicinity of the crack-tip. However, both singular FEM [Zienkiewicz and Taylor (2000)] and singular ES-FEM [Liu *et al.* (2011b)] need extra nodes for the crack tip elements to reproduce the stress singularity in the vicinity of the crack-tip. When dealing with crack propagation problems, constantly adding extra nodes for the crack tip elements and deleting extra nodes for none of the crack tip elements (used to be crack tip elements) are cumbersome. The eES-FEM is free from this issue. eES-FEM is a development of ES-FEM, and very limited change is needed on the ES-FEM code to compose the eES-FEM code. In our future work, we will further develop eES-FEM for crack propagation problems and compare the results with those of singular FEM, singular ES-FEM and XFEM.

3.2. *Edge-based strain smoothing*

In the ES-FEM, we do not calculate the strain in elements by differentiating the displacement; instead, we compute the "smoothed strain" over the smoothing domains. Given the triangular mesh, the edge-based smoothing domains are created by connecting two endpoints of each edge to the centers of the adjacent elements, as shown in Fig. 2. So, we need to label all element edges.

Now we take the smoothing domain Ω_λ created from element edge-λ as an instance. Ω_λ may be a quad or a triangle depending on whether edge-λ is inside the problem domain or on the boundary; see Fig. 3 for the two situations. The average strain over Ω_λ is referred to as the smoothing strain, defined by

$$\overline{\varepsilon}_\lambda = \frac{1}{A_\lambda} \int_{\Omega_\lambda} \varepsilon \mathrm{d}\Omega \tag{17}$$

with A_λ = area of Ω_λ.

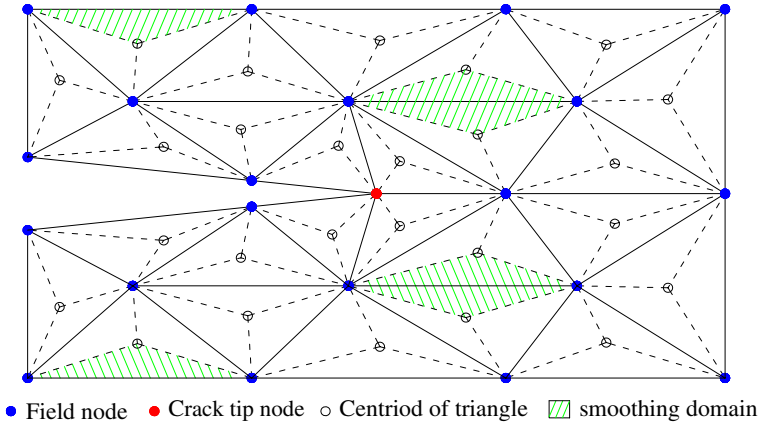

Fig. 2. An ESFEM model: triangular mesh (solid lines), triangular and quadrilateral smoothing domains for fracture problem with an opening crack.

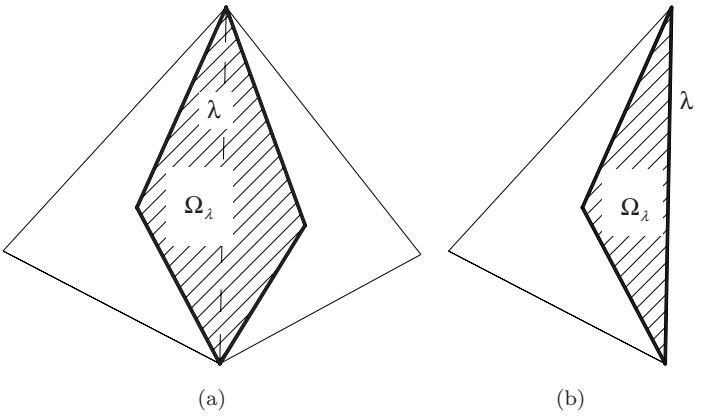

Fig. 3. Smoothing domain from edge-λ. (a) Inner edge and (b) Boundary edge.

By substituting Eq. (3) into Eq. (17) and applying Green's divergence theorem, we have

$$\overline{\boldsymbol{\varepsilon}}_\lambda = \frac{1}{A_\lambda}\int_{\partial\Omega_\lambda} \boldsymbol{L}_n \boldsymbol{u}\mathrm{d}\Gamma, \tag{18}$$

where $\partial\Omega_\lambda$ = boundary of Ω_λ; $\boldsymbol{L}_n$ is the matrix induced by the differential operator ∂ in Eq. (4), defined by

$$\boldsymbol{L}_n = \begin{bmatrix} n_x & 0 \\ 0 & n_y \\ n_y & n_x \end{bmatrix} \tag{19}$$

in which n_x and n_y are x- and y-components of unit outward normal $\boldsymbol{n}$ on $\partial\Omega_\lambda$, respectively.

Now we substitute Eq. (15) in Eq. (18), resulting in

$$\overline{\boldsymbol{\varepsilon}}_\lambda = \overline{\boldsymbol{B}}_\lambda \boldsymbol{a}_\lambda. \tag{20}$$

To explain Eq. (20), we denote by $N[\lambda]$ the set of all nodes that are nodes of elements sharing edge $-\lambda$. Then, $\boldsymbol{a}_\lambda$ = generalized degrees of freedom vector of the nodes of set $N[\lambda]$; the matrix $\overline{\boldsymbol{B}}_\lambda = [\overline{\boldsymbol{B}}_\lambda^j]$, the superscript $j \in N[\lambda]$, and

$$\overline{\boldsymbol{B}}_\lambda^j = \frac{1}{A_\lambda}\int_{\partial\Omega_\lambda} \boldsymbol{L}_n \boldsymbol{N}_j \mathrm{d}\Gamma. \tag{21}$$

3.3. *Generalized Galerkin method and computation of stiffness matrix*

The standard Galerkin formulation of linear elasticity says that $\boldsymbol{u}_h$ solves the problem of interest if and only if

$$a(\boldsymbol{u}_h, \boldsymbol{v}_h) = f(\boldsymbol{v}_h) \tag{22}$$

for any $\boldsymbol{v}_h$; where

$$a(\boldsymbol{u}_h, \boldsymbol{v}_h) = \int_\Omega \boldsymbol{\varepsilon}(\boldsymbol{v}_h) \cdot \boldsymbol{\sigma}(\boldsymbol{u}_h) \mathrm{d}\Omega, \tag{23}$$

$$f(\boldsymbol{v}_h) = \int_\Omega \boldsymbol{b} \cdot \boldsymbol{v}_h \mathrm{d}\Omega + \int_{\Gamma_t} \overline{\boldsymbol{t}} \cdot \boldsymbol{v}_h \mathrm{d}\Gamma. \tag{24}$$

Here and subsequently, we omit the constraints on both $\boldsymbol{u}_h$ and $\boldsymbol{v}_h$. In Eq. (23), $\boldsymbol{\varepsilon}(v_h)$ and $\boldsymbol{\sigma}(\boldsymbol{u}_h)$ are calculated by the relationships of $\boldsymbol{\varepsilon}(\boldsymbol{v}_h) = \partial \boldsymbol{v}_h$ and $\boldsymbol{\sigma}(\boldsymbol{u}_h) = \boldsymbol{D}\boldsymbol{\varepsilon}(\boldsymbol{u}_h)$, respectively. This is the procedure adopted by the standard FEM. In the ES-FEM, however, the strain is not calculated by the relationship of $\boldsymbol{\varepsilon}(\boldsymbol{v}_h) = \partial \boldsymbol{v}_h$ but rather by Eq. (20). To establish the ES-FEM, we start from the generalized Galerkin method [Quarteroni and Valli (1997)], which says $\boldsymbol{u}_h$ solves the problem of interest if and only if

$$a_h(\boldsymbol{u}_h, \boldsymbol{v}_h) = f_h(\boldsymbol{v}_h) \tag{25}$$

for any $\boldsymbol{v}_h$; where $a_h(\boldsymbol{u}_h, \boldsymbol{v}_h)$ and $f_h(\boldsymbol{v}_h)$ should satisfy the conditions in the first Strang lemma, see Quarteroni and Valli [1997] for details. Particular for the ES-FEM,

$$a_h(\boldsymbol{u}_h, \boldsymbol{v}_h) = \int_\Omega \overline{\boldsymbol{\varepsilon}}(\boldsymbol{v}_h) \cdot \overline{\boldsymbol{\sigma}}(\boldsymbol{u}_h) \mathrm{d}\Omega, \tag{26}$$

where $\overline{\boldsymbol{\varepsilon}}(\boldsymbol{v}_h)$ is calculated over the smoothing domains, see Eq. (20), and $\overline{\boldsymbol{\sigma}}(\boldsymbol{u}_h) = \boldsymbol{D}\overline{\boldsymbol{\varepsilon}}(\boldsymbol{u}_h)$; and

$$f_h(\boldsymbol{v}_h) = f(\boldsymbol{v}_h). \tag{27}$$

The variational formulation given here is different from that by Liu and Nguyen-Thoi [2010], who derived the variational formulation of S-FEM from the Hu–Washizu principle.

By assembling the contribution of all smoothing domains to $a_h(\boldsymbol{u}_h, \boldsymbol{v}_h)$, and the contribution of all elements to $f_h(\boldsymbol{v}_h)$, we have the system of linear equations for the eES-FEM,

$$\boldsymbol{K}\boldsymbol{a} = \boldsymbol{p}, \tag{28}$$

where $\boldsymbol{a}$ is the generalized degrees of freedom vector collecting the generalized degrees of freedom of all nodes; and $\boldsymbol{K}$ is the global stiffness matrix to be explained subsequently, and $\boldsymbol{p}$ the load vector defined by

$$\boldsymbol{p} = \int_\Omega \boldsymbol{N}^T \boldsymbol{b} \mathrm{d}\Omega + \int_{\Gamma_u} \boldsymbol{N}^T \boldsymbol{b} \mathrm{d}\Gamma \tag{29}$$

and can be formed as in the FEM.

Now we turn to the assemblage of $\boldsymbol{K}$. We first consider the contribution of a typical smoothing domain Ω_λ to $\boldsymbol{K}$, where Ω_λ corresponds to edge $-\lambda$. According to Eq. (26), a local stiffness matrix, denoted by $\boldsymbol{K}_\lambda$, will be generated from Ω_λ. $\boldsymbol{K}_\lambda$ includes $m \times m$ sub-matrices, with $m = 4$ or 3 depending on the number of nodes

of $N[\lambda]$. A typical sub-matrix in $\boldsymbol{K}_\lambda$, is denoted by $\boldsymbol{K}_\lambda^{ij}$, where subscripts i and j represent any two nodes of $N[\lambda]$. $\boldsymbol{K}_\lambda^{ij}$ is calculated by

$$\boldsymbol{K}_\lambda^{ij} = A_\lambda (\overline{\boldsymbol{B}}_\lambda^i)^T \boldsymbol{D} \overline{\boldsymbol{B}}_\lambda^j \tag{30}$$

with $i, j \in N[\lambda]$; the definition of $\overline{\boldsymbol{B}}_\lambda^i$ and $\overline{\boldsymbol{B}}_\lambda^j$ is given by Eq. (21).

Once $\boldsymbol{K}_\lambda$ is obtained, we assemble all $\boldsymbol{K}_\lambda^{ij}$ onto $\boldsymbol{K}$.

To this point we have not differentiated any shape functions whatsoever in computing $\overline{\boldsymbol{B}}_\lambda^i$ or $\overline{\boldsymbol{B}}_\lambda^j$, thus no singularity of $1/r$ is involved.

3.4. *The structure of global stiffness matrix*

Similar to the standard FEM, sub-matrix $\boldsymbol{K}^{ij}$ in $\boldsymbol{K}$ is a nil matrix unless nodes i and j are relevant. According to the way to form $\boldsymbol{K}$, relevant nodes of node-i consist of nodes of two element groups. The elements of group-1 constitute the star ω_i; while the elements of group-2 are those elements neighboring ω_i each of which shares at least one edge with ω_i. Figure 4 gives an example, the elements of group-2 are shadowed, and all nodes marked by • are relevant to node-i. Therefore, the band of S-FEM is in general larger than that of FEM.

3.5. *Recovery of strain/stress field for ES-FEM*

In FEM, the strain/stress obtained in an element is continuous, and is calculated at the Gauss points in each element. However, this is not the case in the ES-FEM because of the discontinuity of strain at the boundaries of smoothing domains located inside elements [Liu and Nguyen-Thoi (2010)]. Therefore in the ES-FEM, it is essential to create a continuous strain field in each element. The "recovery"

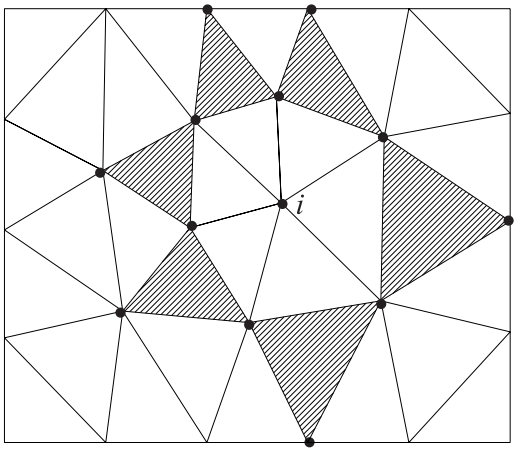

Fig. 4. All nodes marked by • are relevant to node-i.

strain $\overline{\boldsymbol{\varepsilon}}^R$ is continuous inside the element, calculated by

$$\overline{\boldsymbol{\varepsilon}}^R = \sum_{i=1}^{3} L_i \overline{\boldsymbol{\varepsilon}}_i, \tag{31}$$

where $\overline{\boldsymbol{\varepsilon}}_i$ is the average strain at node I, defined as

$$\overline{\boldsymbol{\varepsilon}}_i = \frac{1}{A_i^{ns}} \sum_{\lambda=1}^{n_s^i} A_\lambda \overline{\boldsymbol{\varepsilon}}_\lambda \tag{32}$$

in which n_s^i is the number of smoothing domains Ω_λ around node i, $A_i^{ns} = \sum_{\lambda=1}^{n_s^i} A_\lambda$. Substituting Eq. (31) into Eq. (2) results in the "recovery" stress

$$\overline{\boldsymbol{\sigma}}^R = \boldsymbol{D}\overline{\boldsymbol{\varepsilon}}^R. \tag{33}$$

4. Numerical Examples

In this section, linear fracture examples are analyzed to demonstrate the accuracy of eES-FEM, including fracture of pure mode I, pure mode II and mixed mode. The computation scheme for the SIFs is based on Liu and Nguyen-Thoi [2010]. For comparison purposes, all the problems are also solved using FEM and ES-FEM with the same mesh.

4.1. *Single-edge crack suffered with tensile forces (Mode I)*

The first example is a plate with single-edge crack under the action of a uniform tension on the top surface. The sketch of the problem is shown in Fig. 5 with the parameters $W = 2.0\,\text{m}$, $2H = 6\,\text{m}$, $a = 1\,\text{m}$ and $\sigma = 1.0\,\text{N/m}^2$, Young's modules $E = 1\times10^5\,\text{N/m}^2$ and Poisson's ratio $v = 0.3$. The plane strain condition is assumed.

The value of the mode I SIF K_I as a function of the above parameters is given by Ewalds and Wanhill [1989] as follows

$$K_I = C\sigma\sqrt{a\pi}, \tag{34}$$

where C is the modification factor to reflect the size effect, and if $a/W \leq 0.6$, approximated by

$$C = 1.12 - 0.231\left(\frac{a}{W}\right) + 10.55\left(\frac{a}{W}\right)^2 - 21.72\left(\frac{a}{W}\right)^3 + 30.39\left(\frac{a}{W}\right)^4. \tag{35}$$

Five regular grids are designed to investigate the accuracy and convergence properties of the eES-FEM, with $m \times n = (10\times30, 20\times60, 30\times90, 40\times120, 50\times150)$ elements. Here, $m =$ the number of element layers in x-direction, and $n =$ the number of element layers in y-direction. Figure 6 shows the grid having 341 nodes, 10 element layers in x-direction, and 30 element layers in y-direction.

The normalized SIFs K_I from different grids and different numerical methods are shown in Fig. 7. As can be seen, the computed SIF K_I converges rapidly from below the reference value with elements increasing. In addition, for the same mesh, the solutions of ES-FEM are much better than standard FEM, but the eES-FEM achieves even higher accuracy than the ES-FEM.

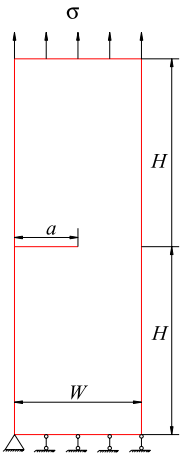

Fig. 5. Finite plate with an edge crack under tension.

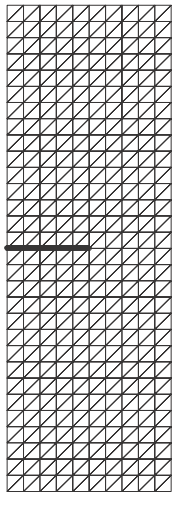

Fig. 6. Mesh with 10 element layers in x-direction for the model in Fig. 5.

4.2. *A plate with a central crack subjected to tensile forces (Mode I)*

As the second example, we consider a rectangular plate of homogeneous isotropic material with a horizontal central crack under the action of uniform tension in the vertical direction. The schematic diagram of the problem is in Fig. 8. Under this setting, the fracture is of pure mode I like example given in Sec. 4.1. The parameters are $W = 15.0\,\text{cm}$, $L = 50.0\,\text{cm}$, $a = 5\,\text{cm}$ and $\sigma = 1\,\text{N/cm}^2$, Young's modules $E = 3\times10^7\,\text{N/cm}^2$ and Poisson's ratio $v = 0.25$. The plane strain condition

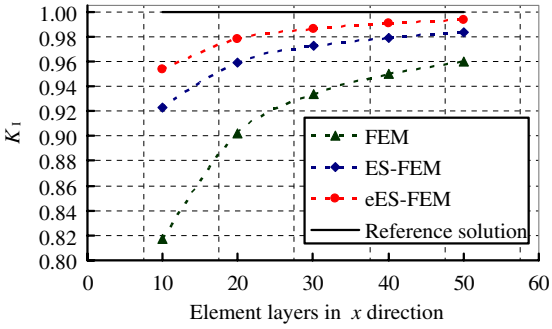

Fig. 7. The normalized SIF K_{I} with different mesh density for single-edge crack suffered with tensile forces.

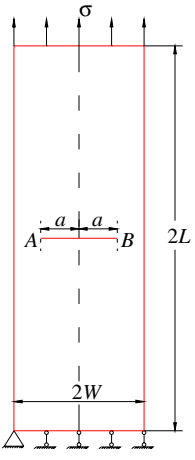

Fig. 8. A rectangular plate with a central crack subjected to tension.

is assumed. The analytical solution of SIFs for such a structure is given by [Tada *et al.* (2000)],

$$K_I = C\sigma\sqrt{a\pi}, \tag{36}$$

where C is the modification factor to reflect the size effect, approximated by

$$C = \left[1 - 0.025\left(\frac{a}{W}\right)^2 - 0.06\left(\frac{a}{W}\right)^4\right]\left(\sec\left(\frac{\pi a}{2W}\right)\right)^{0.5}. \tag{37}$$

For the same purpose as example given in Sec. 4.1, six regular grids are concerned in this analysis with $m \times n = (15 \times 50, 18 \times 60, 21 \times 70, 24 \times 80, 27 \times 90, 30 \times 100)$. Figure 9 shows the grid having 816 nodes, 15 element layers in x-direction, and 50 element layers in y-direction.

Figures 10 and 11 show the normalized SIFs K_{I} for the two crack tips from different grids and different numerical methods. The conclusions drawn in the first example hold as well.

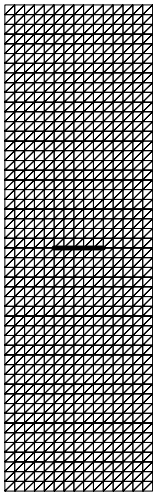

Fig. 9. Mesh with 15 element layers in x-direction for the model in Fig. 8.

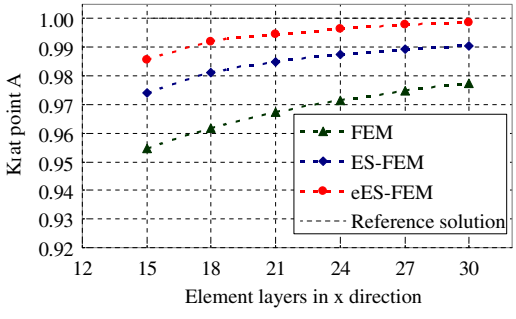

Fig. 10. The normalized SIF K_{I} at crack-tip A with different mesh density for the rectangular plate with a central crack subjected to tension (mode I).

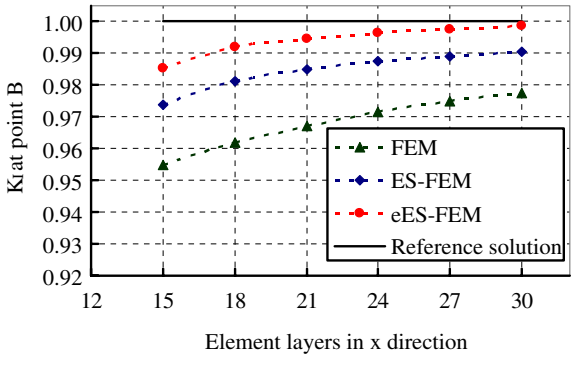

Fig. 11. The normalized SIF K_{I} at crack-tip B with different mesh density for the rectangular plate with a central crack subjected to tension (mode I).

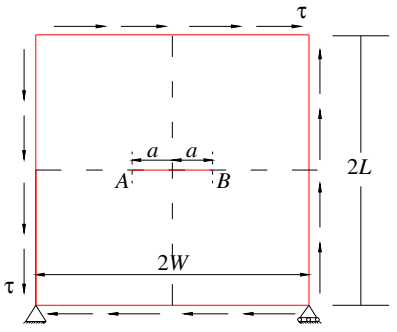

Fig. 12. A rectangular plate with a central crack subjected to shear.

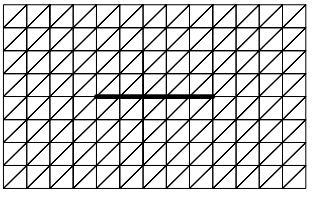

Fig. 13. Mesh (zooming near the crack) for the model in Fig. 12.

4.3. *A plate with a central crack subjected to shear forces (Mode II)*

This example concerns a plate with a horizontal central crack subjected to shear force $\tau = 1\,\mathrm{N/cm^2}$ that gives a pure mode II state, as shown in Fig. 12. The parameters for this problem are $W = 21.0\,\mathrm{cm}$, $L = 22.0\,\mathrm{cm}$ and $a = 2\,\mathrm{cm}$, Young's modules $E = 3\times10^7\,\mathrm{N/cm^2}$ and Poisson's ratio $v = 0.25$. The plane strain condition is assumed. With $W/a \geq 10$, the analytical solution of SIF for such a structure is [Tada *et al.* (2000)]

$$K_{\mathrm{II}} = \tau\sqrt{a\pi}. \tag{38}$$

For the purpose of testing the accuracy and convergence of the eES-FEM, three regular grids ($105\times110, 126\times132, 147\times154$) are designed in this analysis. Figure 13 shows the zooming grid near the crack tip for the 105×110 grid.

Figures 14 and 15 show the normalized SIFs K_{II} for the two crack tips from different grids and different numerical methods. Again, the same conclusions as the first two examples can be drawn.

4.4. *A plate with a central inclined crack (Mixed Mode)*

As the last example, a square plate of homogeneous isotropic material with an inclined crack subjected to a unit tension is considered. The schematic diagram of

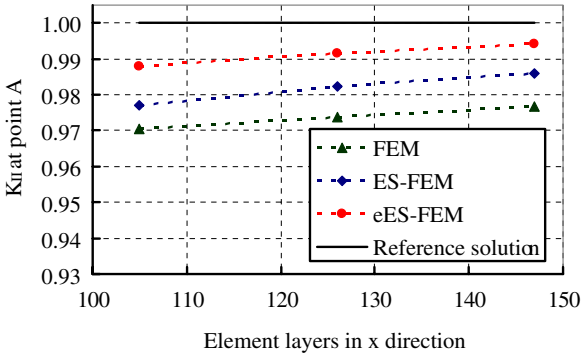

Fig. 14. The normalized SIF K_{II} at crack-tip A with different mesh density for the rectangular plate with a central crack subjected to shear (mode II).

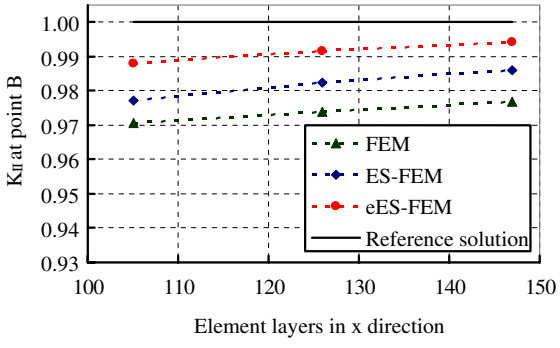

Fig. 15. The normalized SIF K_{II} at crack-tip B with different mesh density for the rectangular plate with a central crack subjected to shear (mode II).

the problem is shown in Fig. 16. Under this setting, the fracture is of mixed mode. The parameters for this problems are $L = 20\,\mathrm{m}$, $a = 1\,\mathrm{m}$, $\sigma = 1\,\mathrm{N/m^2}$, Young's modules $E = 200\,\mathrm{MPa}$ and Poisson's ratio $v = 0.3$. The plane strain condition is assumed. With $L/a \geq 20$, the analytical solution of SIFs as a function of the angle β for this setting are available as [Aliabadi *et al.* (1987)]

$$\begin{cases} K_{\mathrm{I}} = \sigma \cos^2\beta\sqrt{a\pi} \\ K_{\mathrm{II}} = \sigma \sin\beta\cos\beta\sqrt{a\pi} \end{cases}. \tag{39}$$

Four grids with varying β, namely $\beta = 30°$(331 nodes), $40°$(320 nodes), $50°$(331 nodes), $60°$(315 nodes) are designed in this analysis. Figure 17 shows the grid of $\beta = 60°$ and 315 nodes.

The normalized mode I and mode II SIFs by different numerical methods are presented in Figs. 18 to 21. It is observed that best agreement with the reference solution is obtained by the eES-FEM.

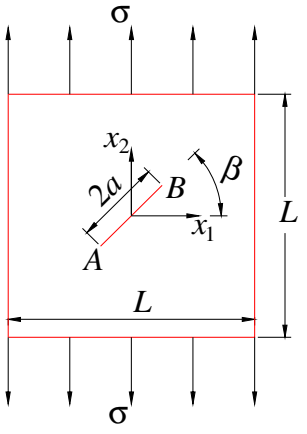

Fig. 16. A square plate with an inclined crack subjected to tension.

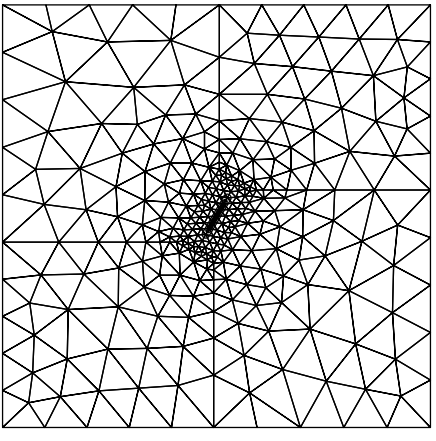

Fig. 17. Mesh used for the square plate with an inclined crack ($\beta = 60°$).

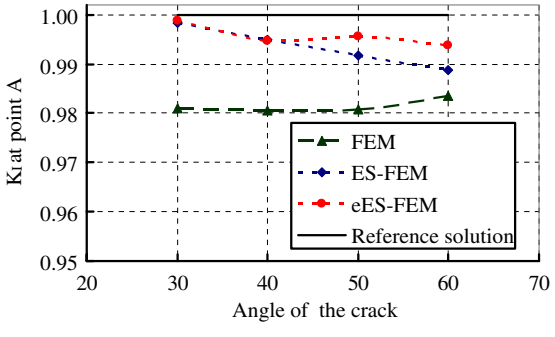

Fig. 18. The normalized SIF K_{I} at crack-tip A with different crack angle for the rectangular plate with a inclined crack subjected to tension (mixed mode).

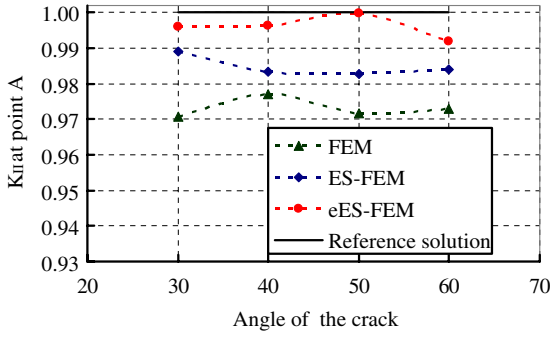

Fig. 19. The normalized SIF K_{II} at crack-tip A with different crack angle for the rectangular plate with a inclined crack subjected to tension (mixed mode).

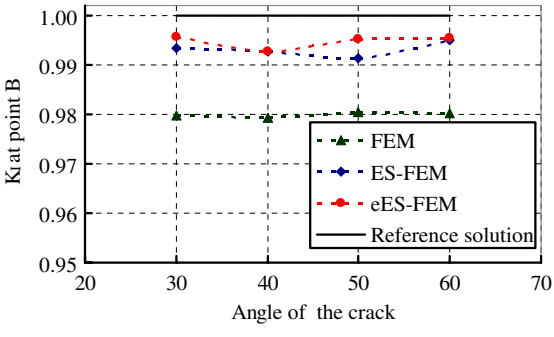

Fig. 20. The normalized SIF K_{I} at crack-tip B with different crack angle for the rectangular plate with a inclined crack subjected to tension (mixed mode).

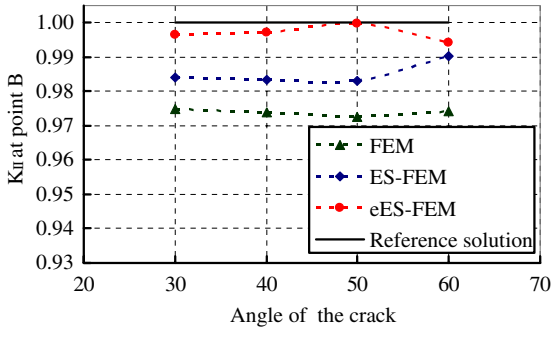

Fig. 21. The normalized SIF K_{II} at crack-tip B with different crack angle for the rectangular plate with a inclined crack subjected to tension (mixed mode).

5. Discussions and Conclusions

The eES-FEM has been developed for linear elastic fracture problems, based on the ES-FEM with triangular meshes. The major items of Williams' displacement series are incorporated to reflect the asymptotic behavior of the solution near the crack tip. The proposed formulation does not differentiate the shape functions in computing the element stiffness matrix. As a result, there is no need to treat the $1/r$ singularity. The complexity of computation is accordingly reduced significantly. Numerical examples indicate that the proposed method converges faster than either ES-FEM or FEM.

To enhance the computational efficiency of the proposed method, the recovery procedure [Nguyen-Xuan *et al.* (2013)] for estimating errors and self-adaptive analysis will be conducted in our coming works.

Acknowledgments

This study is supported by the National Basic Research Program of China (973 Program), under Grant No. 2014CB047100; the National Natural Science Foundation of China, under Grant Nos. 51609240, 11572009 and 51538001.

References

Aliabadi, M. H., Rooke, D. P. and Cartwright, D. J. [1987] "Mixed-mode Bueckner weight functions using boundary element analysis," *Int. J. Fract.* **34**, 131–147.

Babuška, I. and Melenk, J. M. [1997] "The partition of unity method," *Int. J. Numer. Methods Eng.* **40**, 727–758.

Belytschko, T., Gracie, R. and Ventura, G. [2009] "A review of extended/generalized finite element methods for material modelling," *Model. Simulat. Mater. Sci. Eng.* **17**, 043001.

Brighenti, R. [2005] "Application of the element-free Galerkin meshless method to 3-D fracture mechanics problems," *Eng. Fract. Mech.* **72**, 2808–2820.

Chen, J. S., Wu, C. T., Yoon, S. and You, Y. [2001] "Stabilized conforming nodal integration for Galerkin mesh-free methods," *Int. J. Numer. Methods Eng.* **50**, 435–466.

Duflot, M. and Nguyen-Dang, H. [2004] "Fatigue crack growth analysis by an enriched meshless method," *J. Comput. Appl. Math.* **168**, 155–164.

Ewalds, H. and Wanhill, R. [1989] *Fracture Mechanics* (Edward Arnold, New York).

Jiang, Y., Liu, G. R., Zhang, Y. W., Chen, L. and Tay, T. E. [2011] "A singular ES-FEM for plastic fracture mechanics," *Comput. Methods Appl. Mech. Eng.* **200**, 2943–2955.

Leonel, E. D., Chateauneuf, A. and Venturini, W. S. [2012] "Probabilistic crack growth analyses using a boundary element model: Applications in linear elastic fracture and fatigue problems," *Eng. Anal. Bound. Elem.* **36**, 944–959.

Liu, G. R., Jiang, Y., Chen, L., Zhang, G. Y. and Zhang, Y. W. [2011a] "A singular cell-based smoothed radial point interpolation method for fracture problems," *Comput. Struct.* **89**, 1378–1396.

Liu, G. R. and Nguyen-Thoi, T. [2010] *Smoothed Finite Element Methods* (CRC Press, New York).

Liu, G. R., Nourbakhshnia, N. and Zhang, Y. W. [2011b] "A novel singular ES-FEM method for simulating singular stress fields near the crack tips for linear fracture problems," *Eng. Fract. Mech.* **78**, 863–876.

Melenk, J. M. and Babuška, I. [1996] "The partition of unity finite element method: basic theory and applications," *Comput. Methods Appl. Mech. Eng.* **139**, 289–314.

Nguyen-Thanh, N., Rabczuk, T., Nguyen-Xuan, H. and Bordas, S. [2008] "A smoothed finite element method for shell analysis," *Comput. Methods Appl. Mech. Eng.* **198**, 165–177.

Nguyen-Thoi, T., Liu, G. R., Vu-Do, H. C. and Nguyen-Xuan, H. [2009] "An edge-based smoothed finite element method (ES-FEM) for visco-elastoplastic analyses of 2D solids using triangular mesh," *Comput. Mech.* **45**, 23–44.

Nguyen-Xuan, H., Liu, G. R., Bordas, S., Natarajan, S. and Rabczuk, T. [2013] "An adaptive singular ES-FEM for mechanics problems with singular field of arbitrary order," *Comput. Methods Appl. Mech. Eng.* **253**, 252–273.

Nguyen-Xuan, H., Liu, G. R., Nguyen-Thoi, T. and Nguyen-Tran, C. [2009] "An edge-based smoothed finite element method (ES-FEM) for analysis of two-dimensional piezoelectric structures," *Smart Mater. Struct.* **18**, 065015.

Nguyen-Xuan, H., Liu, G. R., Nourbakhshnia, N. and Chen, L. [2012] "A novel singular ES-FEM for crack growth simulation," *Eng. Fract. Mech.* **84**, 41–66.

Nguyen-Xuan, H., Rabczuk, T., Bordas, S. and Debongnie, J. F. [2008] "A smoothed finite element method for plate analysis," *Comput. Methods Appl. Mech. Eng.* **197**, 1184–1203.

Puso, M. A., Chen, J. S., Zywicz, E. and Elmer, W. [2008] "Meshfree and finite element nodal integration methods," *Int. J. Numer. Methods Eng.* **74**, 416–446.

Quarteroni, A. and Valli, A. [1997] *Numerical Approximation of Partial Differential Equations* (Springer-Verlag, Berlin).

Sukumar, N., Chopp, D. L. and Moran, B. [2003] "Extended finite element method and fast marching method for three-dimensional fatigue crack propagation," *Eng. Fract. Mech.* **70**, 29–48.

Tada, H., Paris, P. C. and Irwin, G. R. [2000] *The Stress Analysis of Cracks Handbook* (ASME Press, New York).

Williams, M. L. [1957] "On the stress distribution at the base of a stationary crack," *J. Appl. Mech.* **24**, 109–119.

Yan, X. [2007] "Automated simulation of fatigue crack propagation for two-dimensional linear elastic fracture mechanics problems by boundary element method," *Eng. Fract. Mech.* **74**, 2225–2246.

Zheng, C., Wu, S. C., Tang, X. H. and Zhang, J. H. [2010] "A novel twice-interpolation finite element method for solid mechanics problems," *Acta Mech. Sin.* **26**, 265–278.

Zheng, H. and Xu, D. D. [2014] "New strategies for some issues of numerical manifold method in simulation of crack propagation," *Int. J. Numer. Methods Eng.* **97**, 986–1010.

Zheng, H., Liu, F. and Li, C. G. [2015] "Primal mixed solution to unconfined seepage flow in porous media with numerical manifold method," *Appl. Math. Model.* **39**, 794–808.

Zienkiewicz, O. C. and Taylor, R. L. [2000] *The Finite Element Method*, Fifth Edition (Butterworth Heinemann, Oxford).